ISSN 1674-1056
http://cpb.iphy.ac.cn
http://iopscience.iop.org/cpb
中国物理 B
Chinese Physics
中国物理 Chinese Physics B

Water-based processed and alkoxide-based processed indium oxide thin-film transistors at different annealing temperatures

Xu-Yang Li(栗旭阳), Zhi-Nong Yu(喻志农), Jin Cheng(程锦), Yong-Hua Chen(陈永华), Jian-She Xue(薛建设), Jian Guo(郭建), Wei Xue(薛唯)
Citation: Chin. Phys. B . 2018, 27(4): 048504. **doi:** 10.1088/1674-1056/27/4/048504

Journal homepage: http://cpb.iphy.ac.cn; http://iopscience.iop.org/cpb

What follows is a list of articles you may be interested in

Research on the radiation hardened SOI devices with single-step Si ion implantation

Li-Hua Dai(戴丽华), Da-Wei Bi(毕大炜), Zhi-Yuan Hu(胡志远), Xiao-Nian Liu(刘小年), Meng-Ying Zhang(张梦映), Zheng-Xuan Zhang(张正选), Shi-Chang Zou(邹世昌)
Chin. Phys. B . 2018, 27(4): 048503. **doi:** 10.1088/1674-1056/27/4/048503

Experimental and simulation studies of single-event transient in partially depleted SOI MOSFET

Wei-Wei Yan(闫薇薇), Lin-Chun Gao(高林春), Xiao-Jing Li(李晓静), Fa-Zhan Zhao(赵发展), Chuan-Bin Zeng(曾传滨), Jia-Jun Luo(罗家俊), Zheng-Sheng Han(韩郑生)
Chin. Phys. B . 2017, 26(9): 098505. **doi:** 10.1088/1674-1056/26/9/098505

Intrinsic relationship between photoluminescence and electrical characteristics in modulation Fe-doped AlGaN/GaN HEMTs

Jianfei Li(李建飞), Yuanjie Lv(吕元杰), Changfu Li(李长富), Ziwu Ji(冀子武), Zhiyong Pang(庞智勇), Xiangang Xu(徐现刚), Mingsheng Xu(徐明升)
Chin. Phys. B . 2017, 26(9): 098504. **doi:** 10.1088/1674-1056/26/9/098504

Modeling and understanding of the thermal failure induced by high power microwave in CMOS inverter

Yu-Hang Zhang(张宇航), Chang-Chun Chai(柴常春), Yang Liu(刘阳), Yin-Tang Yang(杨银堂), Chun-Lei Shi(史春蕾), Qing-Yang Fan(樊庆扬), Yu-Qian Liu(刘彧千)
Chin. Phys. B . 2017, 26(5): 058502. **doi:** 10.1088/1674-1056/26/5/058502

Positive gate-bias temperature instability of ZnO thin-film transistor

Liu Yu-Rong, Su Jing, Lai Pei-Tao, Yao Ruo-He
Chin. Phys. B . 2014, 23(6): 068501. **doi:** 10.1088/1674-1056/23/6/068501

Water-based processed and alkoxide-based processed indium oxide thin-film transistors at different annealing temperatures*

Xu-Yang Li(栗旭阳)[1], Zhi-Nong Yu(喻志农)[1,†], Jin Cheng(程锦)[1], Yong-Hua Chen(陈永华)[1], Jian-She Xue(薛建设)[2], Jian Guo(郭建)[1,2], and Wei Xue(薛唯)[1]

[1] *School of Optics and Photonics and Beijing Engineering Research Center of Mixed Reality and Advanced Display, Beijing Institute of Technology, Beijing* 100081, *China*

[2] *Beijing BOE Optoelectronics Technology Co., Ltd, Beijing* 100176, *China*

(Received 2 November 2017; revised manuscript received 18 January 2018; published online 10 March 2018)

In this study, indium oxide (In_2O_3) thin-film transistors (TFTs) are fabricated by two kinds of low temperature solution-processed technologies ($T_a \leq 300$ °C), i.e., water-based (DIW-based) process and alkoxide-based (2-ME-based) process. The thickness values, crystallization properties, chemical structures, surface roughness values, and optical properties of In_2O_3 thin-films and the electrical characteristics of In_2O_3 TFTs are studied at different annealing temperatures. Thermal annealing at higher temperature leads to an increase in the saturation mobility (μ_{sat}) and a negative shift in the threshold voltage (V_{TH}). The DIW-based processed In_2O_3-TFT annealed at 300 °C exhibits excellent device performance, and one annealed at 200 °C exhibits an acceptable μ_{sat} of 0.86 $cm^2/V{\cdot}s$ comparable to that of a-Si:H TFTs, whereas the 2-ME-based TFT annealed at 300 °C exhibits an abundant μ_{sat} of 1.65 cm^2/Vs and one annealed at 200 °C is inactive. The results are attributed to the fact that the DIW-based process induces a higher degree of oxidation and less defect states than the 2-ME-based process at the same temperature. The DIW-based process for fabricating the In_2O_3 TFT opens the way for the development of nontoxic, low-cost, and low-temperature oxide electronics.

Keywords: water-based process, alkoxide-based process, annealing temperature, thin-film transistors

PACS: 85.30.Tv, 78.40.Fy, 81.15.–z **DOI:** 10.1088/1674-1056/27/4/048504

1. Introduction

The development of thin-film transistors (TFTs) based on transparent oxide semiconductors (TOSs) such as zinc oxide (ZnO), indium–zinc oxides (IZO), indium–gallium–zinc oxide (IGZO), and other transparent oxides has attracted a great deal of attention as the next-generation circuitry for displays and energy devices due to their high electron mobility and good transparency in the visible spectral region compared with α-Si:H TFTs.[1–8] Among the methods to fabricate the TOSs, the solution-based process has drawn tremendous research attention due to its low-cost, high-throughput and large area deposition compared with the vacuum-based process. Unfortunately, the traditional solution-processed condensation, densification, and impurity removal typically require a high-temperature annealing step ($T_a > 400$ °C), which is one major obstacle in using flexible substrates to fabricate the devices.[9] In an alkoxide-based precursor solution, the organic solvents have the advantages of good solubility and coating property. However, the removal of the organic group requires additional thermal energy, resulting in high process temperature. To achieve high-performance oxide TFTs at low temperature ($T_a \leq 300$ °C), such methods as sol–gel on a chip,[10] combustion process,[11] deep-ultraviolet photochemical activation,[12] high-pressure annealing under an O_2 atmosphere,[13] doping with suitable dopants,[14] the single precursor and solvent system,[15] and aqueous routes[3] have been investigated. Compared with the above mentioned methods, the water-based process is very appealing for its economic and ecological advantages.

Pure In_2O_3 is a typical n-type TOS material with a wide bandgap of about 3.60 eV–3.75 eV. In particular, the bottom of the conduction band of In_2O_3 consists of the single free electron-like band of In 5s states hybridized with highly dispersed O 2s states, and the valence band edge that arises from the O 2p states hybridized with In 5d states. This unique band structure results in a uniform distribution of the charges and reduces the scattering to a minimum,[16] which makes the In_2O_3 thin-films exhibit high intrinsic mobility. These merits make In_2O_3 a more promising candidate for practical transistors. In the early studies, In_2O_3 thin-films were primarily prepared using vacuum-based processes.[17–19] In recent years, solution processes have been extensively studied.[20–22] In consideration of all these cases, there are few contrastive investigations of water-based processed devices and alkoxide-based processed devices whose performances are dependent on annealing. In fact, as is well known, the precursor solvent and annealing temperature, as the main process parameters,

*Project supported by the National Natural Science Foundation of China (Grant No. 61675024) and the National Basic Research Program of China (Grant No. 2014CB643600).

†Corresponding author. E-mail: znyu@bit.edu.cn

© 2018 Chinese Physical Society and IOP Publishing Ltd

have crucial effects on device performances.

In this paper, considering the practical applications of In_2O_3 thin-films in the electronic industry, we demonstrate here the fabrication of solution-processed In_2O_3 TFTs by using deionized water (DIW) and 2-methoxyethanol (2-ME) as the precursor solvent, respectively. The emphasis of this work is to contrastively investigate the characteristics of TFTs by using water-based (DIW-based) processed and alkoxide-based (2-ME-based) processed In_2O_3 thin-films annealed at different temperatures as the channel layer, respectively. Understanding of the mechanisms responsible for different performances and the different dependence on the annealing temperature for the two approaches would be the main contribution of this paper.

2. Experimental details

2.1. Precursor solution synthesis

All reagents were purchased from Alfa Aesar. The DIW-based and 2-ME-based precursor solutions were synthesized by dissolving 0.2 M $In(NO_3)_3 \cdot xH_2O$ (99.999%) in deionized water (DIW, ACS Reagent) and 2-methoxyethanol (2-ME, 99%), respectively. All the precursor solutions were vigorously stirred for 6 h and aged for 12 h at room temperature to obtain a clear, colorless, and homogeneous solution.

2.2. Fabrication of transistors

A bottom-gate and top-contact device structure was adopted for the DIW-based and 2-ME-based In_2O_3 TFTs. Heavily doped p-type Si wafer with 100 nm thermally grown SiO_2 layer (SiO_2/p^+-Si) was used as the substrate of TFT. The Si wafer and SiO_2 layer served as the gate electrode and dielectric layer of TFT, respectively. Prior to coating, the solutions were filtered through a 0.22 μm syringe filter to remove dust. The SiO_2/p^+-Si substrates were cleaned for 10 min in acetone, ethanol, and DIW in sequence with ultrasonic vibration and dried with blowing nitrogen gas, and then exposed to O_2 plasma for 10 min to enhance the hydrophilicity. The DIW-based In_2O_3 precursor solution and 2-ME-based In_2O_3 precursor solution were spun on the substrates at 4500 rpm for 30 s, and directly placed on a hot plate for pre-annealing at 150 °C for 10 min. After that, the samples were annealed in a muffle furnace at various temperatures (200 °C, 250 °C, 300 °C, 350 °C) under ambient atmosphere for 2 h. For convenience, the DIW-based (2-ME-based) In_2O_3 thin-films annealed at 200 °C, 250 °C, 300 °C, and 350 °C, hereafter, were abbreviated as DIW(2-ME)-200, DIW(2-ME)-250, DIW(2-ME)-300, and DIW(2-ME)-350, respectively. A 100-nm-thick Al thin film was deposited on the In_2O_3 channel layer as source and drain electrodes by thermal evaporation through a shadow mask with a channel length (L) of 100 μm and channel width (W) of 1000 μm. For thin-film performance test, the aforementioned preparation parameters were adopted to fabricate DIW-based and 2-ME-based In_2O_3 thin-films on glass substrates and lightly doped Si substrates, respectively.

2.3. Characteristics of solutions, thin-films, and thin-film transistors

Thermal characteristics of the precursor solutions were performed by thermogravimetric and differential scanning calorimetry (TGA-DSC, Germany, NETZSCH, STA449F3) with a 10-°C/min heating rate up to 400 °C under ambient atmosphere. The thickness values and refractive indices of thin-films were analyzed by a spectroscopic ellipsometer (SE, USA, J. A. Woollam Co, Inc., VASE) with a spectrum response range from 400 nm to 1000 nm. The crystallization properties of thin-films were examined by x-ray diffractometer (XRD, Netherlands, PANalytical, Empyrean) with Cu–Kα radiation at 40 kV and 40 mA over a 2θ range from 10° and 60°. The chemical structures of thin-films were investigated by x-ray photo-electron spectroscopy (XPS, Japan, ULVAC-PHI, Inc., PHI QUANTERA-II SXM) with Al–Kα as x-ray source. The surface morphologies and roughness values of thin-films were observed via atomic force microscopy (AFM. USA. Veeco Instruments Inc. Dimension^{TM} 3100). The optical transmittances of thin-films were investigated in a wavelength range from 200 nm to 800 nm by UV-vis spectrophotometer (Japan, Shimadzu, UV-2550). The current–voltage (I–V) characteristics of TFTs were carried out using a semiconductor parameter analyzer (USA, Keithley, 2612A) under ambient condition. Saturation mobility (μ_{sat}) and subthreshold swing (SS), the TFT performance parameters, were evaluated with the conventional metal–oxide–semiconductor field transistor (MOSFET) model described in Eqs. (1) and (2), the threshold voltage V_{TH} was calculated by fitting a straight line of the square root of I_{DS} versus V_{GS}.[11]

$$\mu_{sat} = \left(\partial\sqrt{I_{DS}}/\partial V_G\right)^2 (2L/WC_i), \quad V_{DS} > V_{GS} - V_{TH}, \tag{1}$$

$$S = dV_G/d(\log I_{SD}), \tag{2}$$

where C_i, W, and L are the capacitance per unit area of the gate insulator, the channel width, and the channel length, respectively.

3. Results and discussion

The combination of metal nitrate and 2-ME or DIW without any additional additives or catalysts provides a simple and unique structure in a solution state. Stable 2-ME-based In_2O_3 precursor solution can be formed by the covalent bonds. As a single precursor in a single solvent system, 2-ME-based In_2O_3 precursor solution can minimize the carbon based impurities, therefore it can be used to fabricate In_2O_3 thin-films at low temperature.[23] Water is an impurity-free solvent with a high

static dielectric constant over 60, which favors the dissociation of ionic species and acts as the σ-donor molecule that serves as a nucleophilic ligand.[24] When the metal nitrate is dissolved in water, the ionized metal cation is solvated by the neighboring water molecule and performs a hydrolysis reaction to produce metal hydroxide, and thus stable DIW-based In_2O_3 precursor solution can be formed by the coordinating bonds and be used to fabricate In_2O_3 thin-films at low temperature.

The thermal behaviors of the (a) DIW-based and (b) 2-ME-based In_2O_3 precursor solutions are analyzed and shown in Fig. 1. Solvent evaporation is identified as an endothermic event for all solutions, with correspondent weight loss above 90%, which occurs below 105 °C and 110 °C for DIW-based and 2-ME-based In_2O_3 precursor solutions, respectively.[25] Because the 2-ME has a higher boiling point than the DIW, the 2-ME-based In_2O_3 precursor solution requires higher temperature than DIW-based In_2O_3 precursor solution to evaporate solvent. The TGA-DSC curve of DIW-based In_2O_3 precursor solution shows a weight loss from 105 °C to 215 °C with two exothermic events at 147 °C and 189 °C, which represent the decomposition of residual nitrate, and the de-hydroxylation and condensation reaction, respectively.[26] The TGA-DSC curve of 2-ME-based In_2O_3 precursor solution shows a weight loss from 110 °C to 325 °C with three exothermic events at 120 °C, 165 °C, and 260 °C, which represent the hydrolysis reaction, the decomposition of residual nitrate, and the de-hydroxylation and condensation reaction, respectively.[27] On the basis of the thermal behaviors, the annealing condition for In_2O_3 thin-film is optimized in a temperature range between 200 °C and 350 °C. The thermal decomposition of DIW-based and 2-ME-based In_2O_3 precursor solutions are completed approximately at 215 °C and 325 °C, respectively. It is found that the final decomposition temperature for DIW-based In_2O_3 precursor solution is lower than that for 2-ME-based In_2O_3 precursor solution, which can be attributed to the fact that the coordination bond between the cation and neighboring aquo ion in DIW-based In_2O_3 precursor solution is relatively weak and easily broken with low thermal energy, compared with the covalent bond in 2-ME-based In_2O_3 precursor solution; in addition, 2-ME needs relatively high temperature to decompose and exclude carbonyl groups approximately at 300 °C.[14]

To confirm the condensation and densification behaviors of In_2O_3 thin-films, spectroscopic ellipsometer measurements were performed. Figures 2(a) and 2(b) show respectively the thickness values and the refractive index values of DIW-based and 2-ME-based In_2O_3 thin-films at different annealing temperatures, which are summarized in Table 1. The thickness of the DIW-based (2-ME-based) In_2O_3 thin-film decreases from 9.52 nm (14.62 nm) to 6.99 nm (12.03 nm) accompanied by the refractive index increasing from 1.786 (1.724) to 1.961 (1.893) as the annealing temperature increases from 200 °C to 350 °C. These results represent that higher annealing temperature creates higher density thin-films with fewer impurities.[13] At a fixed annealing temperature, the DIW-based thin-film shows a larger refractive index than the 2-ME-based sample, indicating that the former has fewer impurities and higher density than the latter, because the film density is positively correlated with the refractive index.[28] The film thickness of the 2-ME-based sample is thicker than that of the DIW-based film due to higher viscosity and organic impurity. The results are in agreement with the TGA-DSC analyses that the decomposition and condensation reaction of 2-ME-based thin-film require higher temperature than that of the DIW-based one.

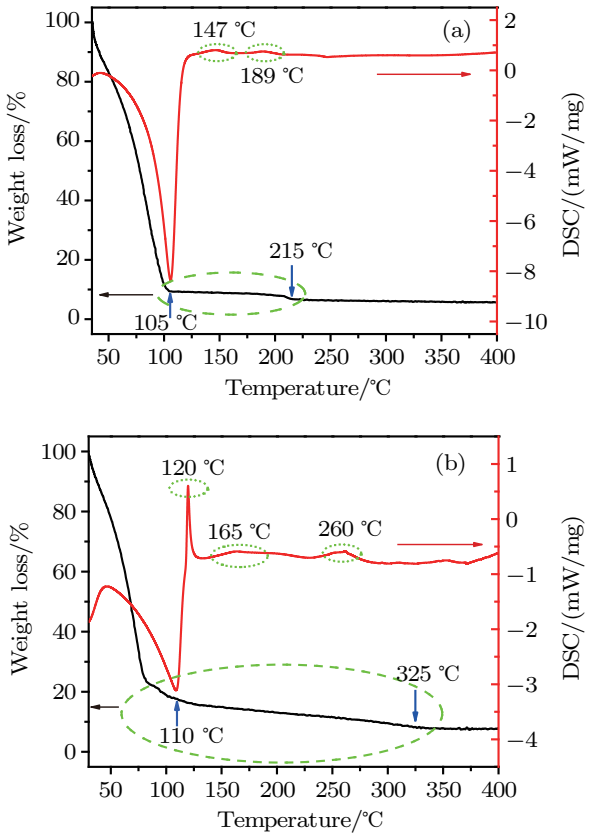


Fig. 1. (color online) TGA-DSC analyses of (a) DIW-based and (b) 2-ME-based In_2O_3 precursor solutions.

Figure 3 shows the crystalline properties of (a) DIW-based and (b) 2-ME-based In_2O_3 thin-films on Si substrates annealed at different annealing temperatures. The results reveal that the DIW-based and the 2-ME-based thin-films are amorphous up to 200 °C and the crystallization behavior occurs at 250 °C. The cubic In_2O_3 phase (JCPDS, No. 65-3170) shows (200), (222), (400), and (440) peaks at 21.5°, 30.6°, 35.5°, and 50.94°, respectively. The sharp peak at 33.1° is attributed to the Si substrate. This result indicates that the DIW-based and 2-ME-based In_2O_3 thin-films have the same crystalline properties.

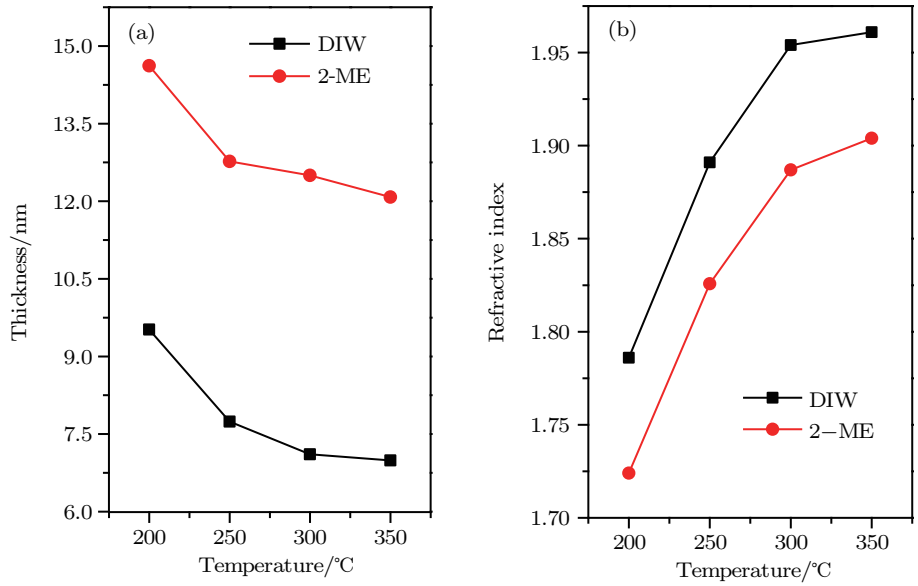


Fig. 2. (color online) Plots of (a) thickness and (b) refractive index versus temperature of DIW-based and 2-ME-based In_2O_3 thin-films at different annealing temperatures.

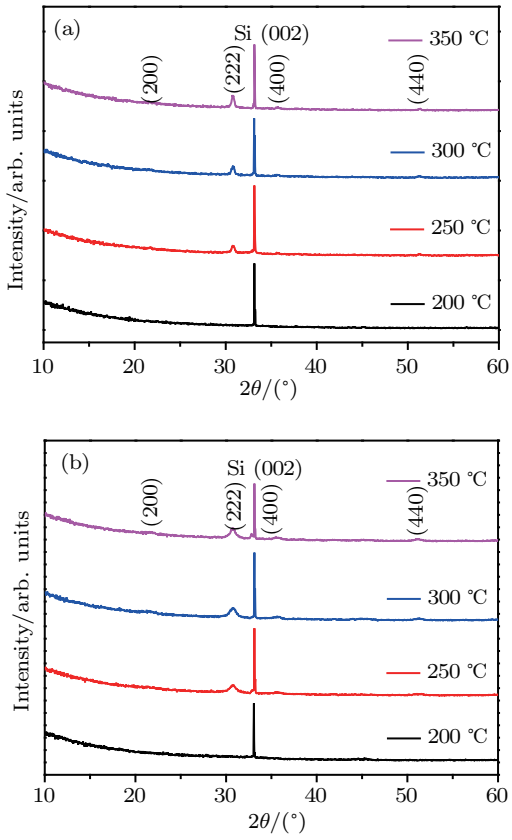


Fig. 3. (color online) XRD patterns of (a) DIW-based and (b) 2-ME-based In_2O_3 thin-films at different annealing temperatures.

Figure 4 shows the XPS O 1s peaks of (a) DIW-based and (b) 2-ME-based In_2O_3 thin-films on Si substrates annealed at different temperatures, and the dependence of (c) the relative peak area of the lattice oxygen (M–O–M) and (d) the mobility of In_2O_3-TFT on annealing temperature. All the XPS peaks are calibrated by taking C 1s reference at 284.6 eV to compensate for any charge-induced shift. The broad asymmetric O 1s signal envelopes of In_2O_3 can be fitted by three nearly Gaussian peaks centered at 529.8±0.1 eV, 531.3±0.1 eV, 532.4±0.1 eV, respectively. The dominant peak centers at 529.8 eV and 531.3 eV could be assigned to M–O–M and either surface or bulk hydroxide species (M–OH), respectively. The peak with the high binding energy component at 532.3 eV could be assigned to surface absorbed oxygen species (e.g., $–CO_3$, H_2O or O_2).[11,22] The relative peak areas of the M–O–M, M–OH, and surface absorbed oxygen species of DIW-based and 2-ME-based In_2O_3 thin-films on Si substrates at different annealing temperatures are calculated and summarized in Table 1. For DIW-based and 2-ME-based In_2O_3 thin-films, as the annealing temperature increases, the relative peak area of the M–O–M significantly increases and those of the M–OH and surface absorbed oxygen species gradually decrease. In addition, for the thin-films annealed at a temperature over 300 °C, only a small quantity of surface absorbed oxygen species ($\leq 5\%$) are indicated by XPS analysis. This phenomenon is mainly because the M–OH bonds and surface absorbed oxygen species are gradually converted into the M–O–M bonds via the thermal-driven condensation process by increasing temperature.

The residual hydroxide groups not forming oxide linkages in the M–O–M network can form the localized defect states, having an electron trapping nature.[15] The conduction band minimum in the metal oxide semiconductor is primarily composed of dispersed vacant s-states with short interaction distance for efficient carrier transport, which can be achieved in ionic oxide but not obviously in hydroxide.[3] Therefore, to maximize the mobility, In_2O_3 thin-film requires an appropriate carrier concentration for percolation conduction and a small number of trap states for the carrier trans-

port, which are represented by increasing the relative peak area of the M–O–M and reducing the relative peak area of the M–OH, respectively.[26] Through the comprehensive analysis of XPS data (Fig. 4), it can be believed that the enhancement of mobility of In_2O_3 TFTs is attributed to the variations of relative peak areas of the M–O–M and M–OH. As shown in Fig. 4(c), the relative peak area of the M–O–M has the order of DIW-350>DIW-300>2-ME-350>2-ME-300>DIW-250>DIW-200>2-ME-250>2-ME-200. The oxidation degree of DIW-based thin-film is higher than the 2-ME-based one at a fixed annealing temperature. Even, the relative peak areas of the M–O–M of 2-ME-350 and 2-ME-250 are smaller than those of DIW-300 and DIW-200, respectively. The results clearly indicate that the residual organic impurities interrupt the formation of M–O–M at low temperature, and the high thermal energy is required for decomposition and M–O–M formation in a 2-ME-based process. Meanwhile, the DIW-based process accelerates M–OH to convert into M–O–M by lowering the activation energy of de-hydroxylation and condensation reaction. These results are consistent with the variation trend of mobility of DIW-based and 2-ME-based In_2O_3 TFTs with different annealing temperatures, which proves the relationships between the mobility and the relative peak areas of the M–O–M and M–OH. In addition, the 2-ME-based In_2O_3 thin-films annealed at 200 °C are primarily composed of M–OH, which indicates that the intermediate compounds do not undergo transformation into M–O–M. This is also in good agreement with the result that the 2-ME-based In_2O_3 TFT is not electrically active at 200 °C.

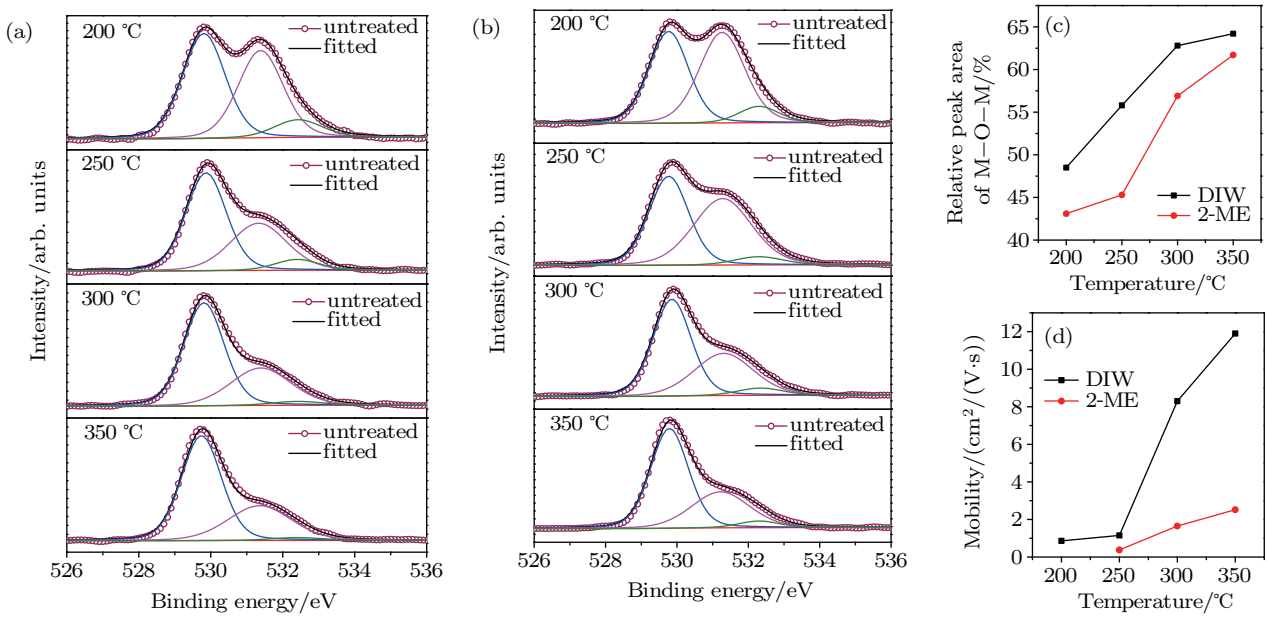


Fig. 4. (color online) XPS data of O 1s analysis of (a) DIW-based and (b) 2-ME-based In_2O_3 thin-films at different annealing temperatures, and the dependence of (c) the relative peak area of the M–O–M and (d) the mobility of In_2O_3-TFT on annealing temperature.

The AFM images of the DIW-based and 2-ME-based In_2O_3 thin-films on SiO_2/p^+-Si substrates annealed at different temperatures are shown in Fig. 5. The root-mean-square (RMS) values of the surface roughness of DIW-200, 2-ME-200, DIW-250, 2-ME-250, DIW-300, 2-ME-300, DIW-350, and 2-ME-350 are 0.161 nm, 0.190 nm, 0.179 nm, 0.271 nm, 0.247 nm, 0.319 nm, 0.254 nm, and 0.329 nm, are shown in Table 1. For DIW-based and 2-ME-based In_2O_3 thin-films, as the annealing temperature increases, the RMS of the surface roughness gradually increases, which is attributed to the slight increase of grain size. The RMS of the surface roughness of 2-ME-based thin-film is higher than that of the DIW-based one at a fixed annealing temperature. The maximum RMS of the surface roughness is only 0.329 nm, which indicates that the DIW-based and 2-ME-based In_2O_3 thin-films are quite smooth and uniform. These small surface roughness values result from the smooth surface of the SiO_2/p+-Si substrate and the ultra-thin film thickness with continuous coverage and negligible porosity.[11]

Figure 7 shows the transfer and output characteristics of TFTs based on DIW-based and 2-ME-based In_2O_3 channel layers at different annealing temperatures. The transfer characteristics are measured using a semiconductor parameter analyzer with a drain voltage (V_{DS}) of +20 V, and gate voltage (V_{GS}) swing from −20 V to 40 V. It is found out that all the devices exhibit n-type behaviors with clear pinch-off and current saturation. In addition, DIW-based and 2-ME-based In_2O_3 TFTs are active at low annealing temperatures of 200 °C and 250 °C, respectively. Except for the inactive 2-ME-based In_2O_3 TFTs annealed at 200 °C, the other TFTs each show a continuous increase in μ_{sat} and a negative shift in V_{TH} with the increase of the annealing temperature. The detailed electrical

characteristics of the DIW-based and 2-ME-based In_2O_3 TFTs are summarized in Table 2.

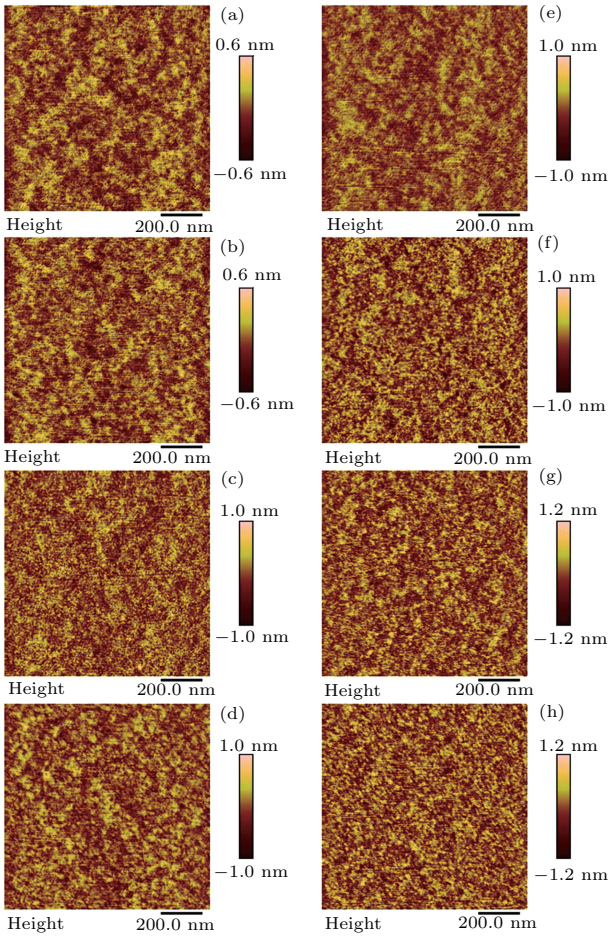


Fig. 5. (color online) AFM morphologies of (a) DIW-200, (b) DIW-250, (c) DIW-300, (d) DIW-350, (e) 2-ME-200, (f) 2-ME-250, (g) 2-ME-300, (h) 2-ME-350.

Transmission optical spectra of DIW-based and 2-ME-based In_2O_3 thin-films on the Corning eagle-2000 glass at different annealing temperatures are shown in Fig. 6. All the thin-films show high optical transparencies in the visible region with the transmittances over 90%.

It is known that the de-hydroxylation reaction at high annealing temperature could lead to the creation of charge carriers in the channel layers,[3] and the carrier transport in semiconductor film is governed by percolation conduction over trap states and is enhanced at high carrier concentration by filling the trap states.[26] The mobility of the semiconductor channel layers together with the electrical performance of as-integrated TFTs depend on the carrier concentration. As a result, the gradual increase of the μ_{sat} value can be attributed to the formation of the M–O–M as well as the decomposition of the M–OH with the increasing annealing temperature.[14] Meanwhile, the negative shift in V_{TH} is due to the high intrinsic carrier concentration for the thin-film annealed at high temperature and few lattice defects acting as carrier traps. Consequently, a small gate voltage is required to induce carriers to prefill the traps, leading to the decrease of V_{TH}.[15]

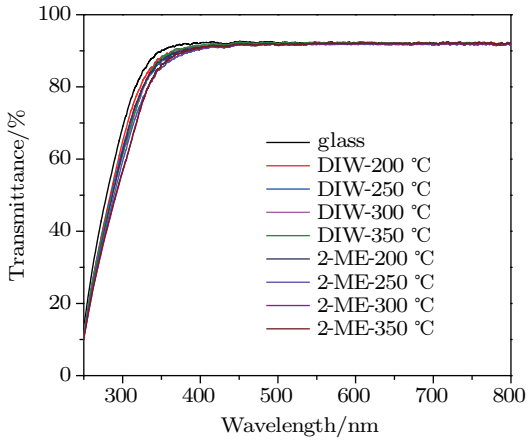


Fig. 6. (color online) Transmission optical spectra of DI-In_2O_3 and 2-ME-In_2O_3 thin films on Corning eagle-2000 glass at different annealing temperatures.

Comparing the electrical properties of the DIW-based and 2-ME-based In_2O_3 TFTs annealed at the same condition, the DIW-based In_2O_3 TFTs show significant mobility increase and V_{TH} negative shift, and the 2-ME-based In_2O_3 TFTs display the distinct falls of both mobility increase and V_{TH} negative shift. In addition, for the 2-ME-based In_2O_3 TFTs annealed at 250 °C and 300 °C, the negative slope of the output characteristic curves are observed in the saturation region as shown in Fig. 7(d), which indicates that lots of electrons are trapped within the In_2O_3 thin-film. The trapped charges act as scattering centers for electrons, thus reducing the saturation current.[29]

Table 1. Summary of the thickness values, the refractive indices, and the relative peak areas of the M–O–M, M–OH, and absorbed oxygen species of DIW-based and 2-ME-based In_2O_3 thin-films on Si substrates at different annealing temperatures.

Solvent	Annealing temperature/°C	Thickness/nm	Refractive index	M–O–M/%	M–OH/%	Absorbed oxygen/%	RMS/nm
DIW	200	9.52	1.786	48.5	42.4	9.1	0.161
DIW	250	7.74	1.891	55.8	37.5	6.7	0.179
DIW	300	7.11	1.954	62.8	34.2	3.0	0.247
DIW	350	6.99	1.961	64.2	33.6	2.2	0.254
2-ME	200	14.62	1.724	43.1	49.1	7.8	0.190
2-ME	250	12.77	1.836	45.3	49.6	5.1	0.271
2-ME	300	12.50	1.887	56.9	38.1	5.0	0.319
2-ME	350	12.03	1.893	61.7	33.9	4.4	0.329

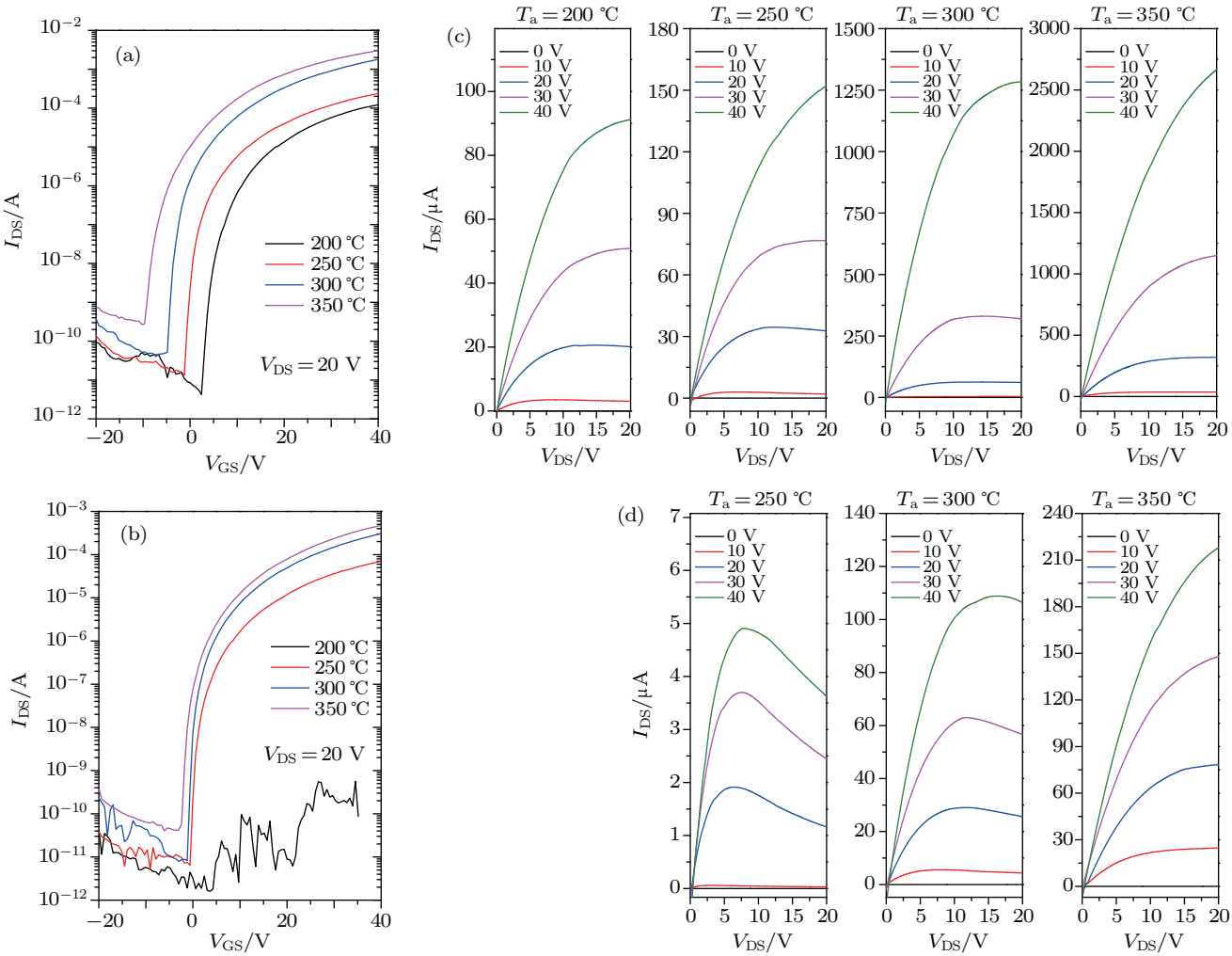


Fig. 7. (color online) Transfer characteristics of TFTs based on (a) DIW-based and (b) 2-ME-based In_2O_3 channel layers at different annealing temperatures. The output characteristics of TFTs based on (c) DIW-based and (d) 2-ME-based In_2O_3 channel layers at different annealing temperatures.

Table 2. Electrical properties of TFTs.

Solvent	Annealing temperature/°C	μ_{sat}/(cm^2/V·s)	I_{on}/I_{off}	V_{TH}/V	SS/(V/dec)	V_{on}/V
DIW-IO	200	0.86	9.10×10^6	10.48	0.44	3.03
DIW-IO	250	1.15	1.96×10^6	5.61	0.55	–1.82
DIW-IO	300	8.30	1.89×10^8	4.73	0.64	–6.67
DIW-IO	350	11.90	1.08×10^7	1.06	0.86	–9.70
2-ME-IO	200	–	–	–	–	–
2-ME-IO	250	0.38	7.29×10^5	7.20	0.82	–0.61
2-ME-IO	300	1.65	3.31×10^7	7.08	0.41	–1.21
2-ME-IO	350	2.52	1.08×10^7	6.73	0.55	–3.64
DIW-I_5Z_2O	300	2.55	1.21×10^7	3.53	0.46	–2.50
DIW- $I_5G_1Z_2O$	300	1.79	6.25×10^7	3.45	0.35	–3.00

It can be clearly seen from Table 2 that the 2-ME-based In_2O_3 TFT at 300 °C exhibits excellent device performances, including abundant μ_{sat} of 1.65 cm^2/V·s, SS of 0.41 V/dec, V_{TH} of 7.08 V, and on/off current ratio of 3.31×10^7. Comparatively, the DIW-based In_2O_3 TFT annealed at 200 °C exhibits an acceptable μ_{sat} of 0.86 cm^2/V·s comparable to that of α-Si:H TFTs,[10] and the DIW-based In_2O_3 TFT annealed at 300 °C presents excellent device performances, consisting of distinguished μ_{sat} of 8.3 cm^2/V·s which is 5 times that of the 2-ME-based In_2O_3 TFT at the same annealing temperature, SS of 0.64 V/dec, V_{TH} of 4.73 V, and on/off current ratio of 1.89×10^8.

In this study, both the DIW-based and 2-ME-based In_2O_3 TFT exhibit acceptable μ_{sat} values (larger than 1 cm^2/V·s,) and on/off current ratio of (larger than 1×10^6) at annealing temperature (T_a = 300 °C): these characteristics are suf-

ficient for display and basic circuitry applications. Especially, the electrical performance of the DIW-based In_2O_3 TFT annealed at 250 °C exhibits an acceptable saturation mobility of 1.15 $cm^2/V{\cdot}s$ and on/off current ratio of 1.96×10^6, which indicates that the DIW-based process allows the fabrication of In_2O_3 TFT at much lower temperature than the 2-ME-based process.

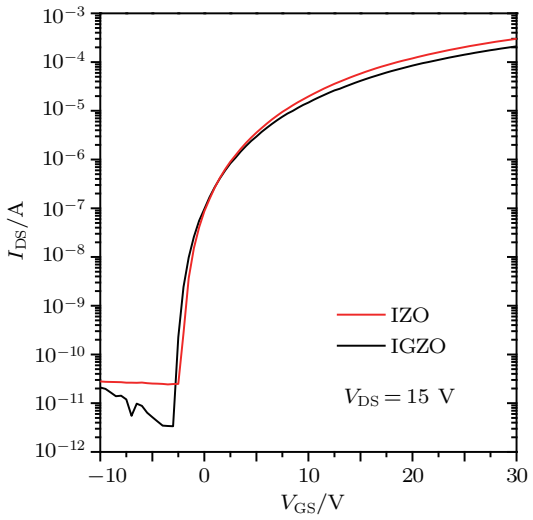


Fig. 8. (color online) Transfer characteristics of IZO and IGZO TFTs.

Finally, we fabricate indium zine oxide (I_5Z_2O) and indium gallium zine oxide ($I_5G_1Z_2O$) TFTs via DIW-based process at an annealing temperature of 300 °C. The transfer characteristics of IZO and IGZO TFTs are shown in Fig. 8. The IZO-TFT and IGZO-TFT annealed at 300 °C exhibit acceptable μ_{sat} values of 2.55 $cm^2/V{\cdot}s$ and 1.79 $cm^2/V{\cdot}s$, respectively.

4. Conclusions

In conclusion, the performances of In_2O_3 thin-films and TFTs fabricated by the DIW-based process and 2-ME-based process are investigated as a function of the annealing temperature. All thin-films show higher density, higher degree of oxidation and less defect states as the annealing temperature increases. In addition, all thin-films have quite smooth and uniform surfaces and high optical transparencies. All TFTs show a continuous increase in μ_{sat} and a negative shift in V_{TH} as the annealing temperature increases. The DIW-based processed and 2-ME-based processed In_2O_3-TFTs annealed at 300 °C exhibit excellent device performances, and the former shows μ_{sat} of 8.3 $cm^2/V{\cdot}s$ which is 5 times that of the latter (μ_{sat} of 1.65 $cm^2/V{\cdot}s$). The DIW-based processed TFT annealed at 200 °C exhibits an acceptable μ_{sat} of 0.86 $cm^2/V{\cdot}s$ comparable to that of α-Si:H TFTs, whereas the 2-ME-based processed In_2O_3-TFT annealed at 200 °C is inactive. These results suggest that the DIW-based and 2-ME-based processed In_2O_3-TFTs could potentially be used for fabricating the low-cost, low-temperature, and high-performance electronic devices. Especially, the DIW-based process could fabricate In_2O_3 thin-film at an annealing temperature as low as 200 °C, which reveals a feasible route to the development of nontoxic, low-cost, and low-temperature oxide electronics.

References

[1] Wager J F 2003 *Science* **300** 1245
[2] Zhang Y H, Mei Z X, Liang H L and Du X L 2017 *Chin. Phys. B* **26** 047307
[3] Liu G X, Liu A, Zhu H H, Shin B, Fortunato E, Martins R, Wang Y Q and Shan F K 2015 *Adv. Funct. Mater.* **25** 2564
[4] Nomura K, Ohta H, Takagi A, Kamiya T, Hirano M and Hosono H 2004 *Nature* **432** 488
[5] Zhang Y H, Mei Z X, Liang H L and Du X L 2017 *Chin. Phys. B* **26** 047307
[6] Park H W, Park K, Kwon J Y, Choi D and Chung K B 2017 *IEEE. Trans. Electron. Dev.* **64** 159
[7] Wu S H, Zhang N, Hu Y S, Chen H, Jiang D P and Liu X Y 2015 *Chin. Phys. B* **24** 108504
[8] Zhang S Y, Yu Z N, Cheng J, Wu D L, Li X Y and Xue W 2016 *Acta Phys. Sin.* **65** 128502 (in Chinese)
[9] Xu W, Cao H, Liang L and Xu J B 2015 *ACS Appl. Mater. Inter.* **7** 14720
[10] Banger K K, Yamashita Y, Mori K, Peterson R L, Leedham T, Rickard J and Sirringhaus H 2011 *Nat. Mater.* **10** 45
[11] Kim M G, Kanatzidis M G, Facchetti A and Marks T J 2011 *Nat. Mater.* **10** 382
[12] Kim Y H, Heo J S, Kim T H, Park S, Yoon M H, Kim J, Oh M S, Yi G R, Noh Y Y and Park S K 2012 *Nature.* **489** 128
[13] Rim Y S, Jeong W H, Kim D L, Lim H S, Kim K M and Kim H J 2012 *J. Mater. Chem.* **22** 12491
[14] Park J H, Yoo Y B, Lee K H, Jang W S, Oh J Y, Chae S S, Lee H W, Han S W and Baik H K 2013 *ACS Appl. Mater. Inter.* **5** 8067
[15] Meng Y, Liu G X, Liu A, Song H, Hou Y, Shin B and Shan F K 2015 *RSC Adv.* **5** 37807
[16] Moses Ezhil Raj A, Lalithambika K C, Vidhya V S, Rajagopal G, Thayumanavan A, Jayachandran M and Sanjeeviraja C 2007 *Physica B* **403** 544
[17] Zhang H Z, Cao H T, Chen A H, Liang L Y, Liu Z M and Wan Q 2010 *Solid. State. Electron.* **54** 479
[18] Yuan Z J, Zhu X M, Wang X, Cai X K, Zhang B P, Qiu D J and Wu H Z 2011 *Thin Solid Films* **519** 3254
[19] Cho S 2012 *Microelectron. Eng.* **89** 84
[20] Leppaniemi J, Huttunen O H, Majumdar H and Alastalo A 2015 *Adv. Mater.* **27** 7168
[21] Kang C M, Kim H, Oh Y W, Baek K H and Do L M 2016 *IEEE. Electron. Dev. Lett.* **37** 595
[22] Kim B S and Kim H J 2016 *IEEE. Trans. Electron. Dev.* **63** 3558
[23] Lee J S, Kwack Y J and Choi W S 2013 *ACS Appl. Mater. Inter.* **5** 11578
[24] Bae B S, Hwang Y H, Seo J S and Choi G M 2013 *ECS Trans.* **50** 101
[25] Branquinho R, Salgueiro D, Santos L, Barquinha P, Pereira L, Martins R and Fortunato E 2014 *ACS Appl. Mater. Inter.* **6** 19592
[26] Liu A, Liu G, Zhu H H, Shin B, Fortunato E, Martins R and Shan F K 2015 *RSC Adv.* **5** 86606
[27] Kwon J M, Jung J, Rim Y S, Kim D L and Kim H J 2014 *ACS Appl. Mater. Inter.* **6** 3371
[28] Jerman M., Qiao Z H and Mergel D 2005 *Appl. Opt.* **44** 3006
[29] Zhang W P, Chen S, Qian S B and Ding S J 2014 *Semicond. Sci. Technol.* **30** 015003